Near-Edge X-Ray Absorption Fine Structures Revealed in Core Ionization Photoelectron Spectroscopy

M. Nakano,[1,2] P. Selles,[3,4] P. Lablanquie,[3,4] Y. Hikosaka,[5] F. Penent,[3,4] E. Shigemasa,[6] K. Ito,[2] and S. Carniato[3,4,*]

[1]*Department of Chemistry, Tokyo Institute of Technology, Tokyo 152855, Japan*
[2]*Institute of Material Structural Science, Photon Factory, Tsukuba, Ibaraki 3050801, Japan*
[3]*UPMC Université Paris 6, UMR 7614, Laboratoire de Chimie Physique-Matière et Rayonnement, 11 rue Pierre et Marie Curie, 75231 Paris Cedex 05, France*
[4]*CNRS, LCPMR(UMR 7614), 11 rue Pierre et Marie Curie, 75231 Parix Cedex 05, France*
[5]*Department of Environmental Science, Niigata University, Niigata 950-2181, Japan*
[6]*UVSOR Facility, Institute for Molecular Science, Okazaki 444-8585, Japan*

(Received 25 April 2013; published 20 September 2013)

Simultaneous core ionization and core excitation have been observed in the C_2H_{2n} ($n = 1, 2, 3$) molecular series using synchrotron radiation and a magnetic bottle time-of-flight electron spectrometer. Rich satellite patterns corresponding to ($K^{-2}V$) core excited states of the K^{-1} molecular ions have been identified by detecting in coincidence the photoelectron with the two Auger electrons resulting from the double core hole relaxation. A theoretical model is proposed providing absolute photoionization cross sections and revealing clear signatures of direct (monopolar) and conjugate (dipolar near-edge x-ray absorption fine structure) shakeup lines of comparable magnitude.

DOI: 10.1103/PhysRevLett.111.123001 PACS numbers: 33.60.+q, 31.10.+z, 32.80.Aa, 33.70.−w

X-ray photoelectron spectroscopy (XPS) and near-edge x-ray absorption fine structure spectroscopy (NEXAFS) are nowadays two routine techniques to determine the composition, chemical state, and electronic structures of atoms, molecules, and solids (see Refs. [1,2]). In XPS, the photoelectron spectra exhibit characteristic peaks at kinetic energies given by the difference between the (fixed) photon energy and the energies of the final ionic states. In NEXAFS spectroscopy, the absorption signal is recorded by varying the photon energy close to an inner-shell threshold. It is dominated by narrow resonances corresponding to the excitation of inner-shell electrons to unoccupied molecular orbitals. Although main features in XPS and NEXAFS correspond to the ionization or excitation of a single electron, the possibility that absorption of a single photon leads to the simultaneous ionization of a core electron and excitation of a valence electron has, however, attracted much interest since the first gas phase electron spectroscopy for chemical analysis studies by Siegbahn and co-workers [1]. The so-called K^{-1} photoelectron shakeup satellite spectra generated by this mechanism have long been interpreted using the sudden approximation [3], in connection with the relaxation of the system after the formation of an inner-shell hole. Evidence for the failure of this model close to the ionization threshold emerged with the observation of photoelectron states forbidden by the sudden approximation monopole selection rules [4]. A mechanism named "conjugate shakeup" was then proposed [5] to describe the formation of such states. In this mechanism, it is the valence electron which is photoexcited while the core electron is ionized in a shake-off process. Since that time, K^{-1} XPS studies have been dedicated to assigning the nature of the shakeup processes (direct or conjugate) [6–13] through examination of the energy dependence of satellite cross sections and, later on, of electron angular distributions.

On the theoretical side, calculation of K^{-1} satellite states is still a challenging subject, as it demands to take into account accurately orbital reorganization effects and electron-electron correlations [14,15]. Sophisticated models have been developed for atoms [16] and molecules [17–22]. Among all these models, only the oldest one [17] studied the formation of conjugate satellites, while the other ones calculated only direct shakeup satellite intensities within the sudden approximation as overlap integrals between initial frozen and final relaxed ($N - 1$) electron states.

In this Letter, we address $K^{-2}V$ processes corresponding to single photon simultaneous core ionization and core excitation in C_2H_{2n} ($n = 1, 2, 3$). These processes can be considered as generating "exotic" highly excited K^{-1} satellites where the electron excited to a valence orbital originates from the same core K orbital. A great effort has been recently devoted to observe K-shell double core hole (DCH) states using either x-ray free electron lasers or synchrotron sources [23–28]. The signature of $K^{-2}V$ states was observed in NH_3 and H_2O [28,29]. Although electronic configurations were computed in the latter case, the intensities have not been calculated yet.

Our experimental XPS satellite patterns recorded for the C_2H_{2n} series are accurate enough to reveal direct and conjugate shakeup satellites of comparable magnitude. Moreover, evolution of these satellites within the molecular series shows surprisingly clear signatures of NEXAFS spectroscopy [2]. In a simplified two active electron model, as that suggested in Fig. 1, $K^{-2}V$ states can be reached by

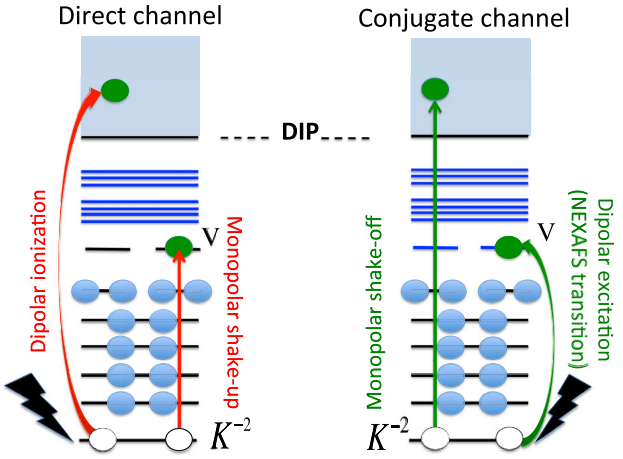

FIG. 1 (color online). Schematic picture of the single photon $K^{-2}V$ direct (left panel) and conjugate (right panel) channels in C_2H_2. In the direct channel, dipolar ionization is accompanied by core to valence monopolar shakeup. In the conjugate channel, core to valence dipolar excitation (NEXAFS-transition) is accompanied by monopolar shake-off.

two alternative paths: either the photon ionizes one K-shell electron (the remaining K-shell electron being shaken up to a vacant orbital V) or the photon excites one K-shell electron to a vacant orbital V (the remaining K-shell electron being shaken off). The first path corresponds to the direct channel where valence states are reached by monopolar transitions, while the second path corresponds to the conjugate channel where valence states are reached by dipolar transitions, as they do in NEXAFS spectroscopy. In both channels, the photon energy is shared between the two electrons, so that NEXAFS transitions can be observed for a fixed photon energy, contrary to regular NEXAFS transitions where a resonant condition is required for photon energy.

A comprehensive theoretical model, developed beyond the sudden approximation routinely implemented in K^{-1} satellite studies, has been built. This model, based on configuration interaction, is likely to reproduce not only the origin of both the main (K^{-2}) and satellite ($K^{-2}V$ or $K^{-2}V^{-1}V'$) lines obtained in ionization by a single photon but also their intensities. Cross sections were evaluated in the dipole approximation from the transition amplitudes calculated in the length gauge. Their expression in atomic units is given by

$$\sigma_{f0} = \frac{2}{3} \times 4\pi^2 \alpha \omega \sum_f \rho(\epsilon_f) \sum_\mu |T_{f0}^{(\mu)}|^2, \quad (1)$$

$$T_{f0}^{(\mu)} = \langle \Psi_f^N | \sum_{k=1}^{N} r_k^{(\mu)} | \Psi_0^N \rangle. \quad (2)$$

Ψ_0^N and Ψ_f^N are the wave functions for the N-electron initial and final states, respectively, and $r_k^{(\mu)}$ are the coordinates of the individual electrons. The factor $2/3$ takes into account the degeneracy due to the possible localization of the double core hole on an A or B carbon atom and the average over molecular orientations. The energy density of final states $\rho(\epsilon_f)$ depends on the photoelectron energy $\epsilon_f = \omega - \mathrm{BE}_f$, BE_f being the binding energy of the $K^{-2}V$ final ionic state. Each final state was approximated by an antisymmetrized superposition where channel couplings in the continuum are neglected. Following the creation and annihilation operator formalism as described in Refs. [30,31], each final state can be written as

$$|\Psi_f^N\rangle = \hat{a}_\epsilon^\dagger |\Psi_f^{N-1}\rangle, \quad (3)$$

where Ψ_f^{N-1} is a bound eigenstate of the residual ion, and $\hat{a}_\epsilon^\dagger$ is the operator for the creation of a continuum state $|\epsilon_f\rangle$. Introducing the product state (3) in the transition amplitude (2), a separation into bound and continuum states appears,

$$T_{f0}^{\mu} = \sum_\ell [d_{\epsilon\ell}^{(\mu)} S_\ell + D_\ell^{(\mu)} s_{\epsilon\ell}], \quad (4)$$

with the following dipole matrix elements and overlaps:

$$d_{\epsilon\ell}^{(\mu)} = \langle \epsilon_f | r^{(\mu)} | \varphi_\ell \rangle, \qquad S_\ell = \langle \Psi_f^{N-1} | \hat{a}_\ell \Psi_0^N \rangle, \quad (5)$$

$$D_\ell^{(\mu)} = \left\langle \Psi_f^{N-1} \left| \sum_k r_k^{(\mu)} \right| \hat{a}_\ell \Psi_o^N \right\rangle, \quad s_{\epsilon\ell} = \langle \epsilon_f | \varphi_\ell \rangle. \quad (6)$$

The operator $\hat{a}_\ell$ annihilates the molecular orbital $|\varphi_\ell\rangle$. The first product in Eq. (4) corresponds to the so-called direct shakeup contribution while the second one corresponds to the conjugate shakeup contribution.

Computations of $D_\ell^{(\mu)}$ and S_ℓ elements were carried out using an original post-Hartree-Fock configuration interaction package, where a common set of Hartree-Fock-self consistent field orthogonal molecular orbitals optimized for the C K^{-1} singly ionized molecule was used. As an example, the initial C_2H_2 ground state was built from the closed-shell configuration $[\sigma_A^2 \sigma_B^2 3\sigma^2 4\sigma^2 1\pi^4 5\sigma^2]$ and included single- and double-valence excitations, as well as minor contributions from core excited configurations and double core-valence excited configurations. The $K^{-2}V$ final states were generated by core ionization of these core excited configurations.

Moreover, in order to take into account accurately relaxation of the valence orbitals in the presence of the double core hole, the basis usually designed to describe the carbon atom [32] was augmented by ($3s$, $3p$, $3d$) diffuse wave functions while the unperturbed carbon atom and the hydrogen atoms were described by a 6-311G^* basis set. To reduce the computational cost of the calculations, all the continuum wave functions were taken to be those associated with the final $K^{-2}V$ state, where V is the lowest unoccupied molecular orbital (LUMO). They were generated from a one-electron static exchange Hamiltonian [33–35] associated with a Stieljes imaging procedure [36–38]. This method also provided a representation of the double K^{-2} continuum. Calculations were performed using a large augmented correlation-consistent polarized valence quintuple zeta basis set centered on C and H atoms [39]. The same large augmented

basis was used to optimize the initial molecular orbitals taking part in the $d^{(\mu)}_{\epsilon\ell}$ and $s_{\epsilon\ell}$ elements.

Experiments were performed at the undulator beam line BL-16A [40] of the Photon Factory, operated in the single-bunch mode. The monochromator entrance and exit slits were adjusted at 50 μm to give a resolving power $h\nu/\Delta h\nu$ of ~5000. A magnetic bottle time-of-flight electron spectrometer [41] was used to collect multicoincidence data sets. The detailed description of the spectrometer and of the data acquisition scheme has been given elsewhere [42]. Electron detection efficiencies were calibrated by measuring Ar $2p$ or Kr $3d$ Auger spectra, alone or in coincidence with photoelectrons, and were found to be about 70% below 200 eV and decrease slowly with increasing electron energy to a value of 50% around 500 eV.

Figure 2 shows experimental evidence for $K^{-2}V$ states in C_2H_2. Their formation and decay are described by

$$\begin{aligned} C_2H_2 + h\nu &\rightarrow C_2H_2^+(K^{-2}V) + e_p \\ &\rightarrow C_2H_2^{2+}(K^{-1}\upsilon^{-2}V) + e_{A_1} \\ &\rightarrow C_2H_2^{3+}(\upsilon^{-4}V) + e_{A_2}, \end{aligned} \tag{7}$$

where υ is a valence shell. The $K^{-2}V$ states are expected to decay sequentially in a similar way as the K^{-2} DCHs do. Thus, the energies of the two released Auger electrons e_{A_i} are predicted to be similar to those (~ 300 eV, ~240 eV) characteristics of the decay of K^{-2} DCHs [43], but slightly higher (a few eV) due to the screening of the spectator V electron. The signal displayed in Fig. 2 shows the energy correlation between two of the electrons when the third one lies in the 200–260 eV energy range (which corresponds to the expected energy range of the Auger electron e_{A_2} released in the last step). The islands around $(x, y) =$ (300 eV, 130 eV) correspond to the (e_{A_1}, e_p) pair and reveal the $K^{-2}V$ states. Two main spots are clearly visible. The vertical strip at ($x = 300$ eV, $y < 118$ eV) corresponds to the core double-photoionization process:

$$\begin{aligned} C_2H_2 + h\nu &\rightarrow C_2H_2^{2+}(K^{-2}) + e_{p_1} + e_{p_2} \\ &\rightarrow C_2H_2^{3+}(K^{-1}\upsilon^{-2}) + e_{A_1} \\ &\rightarrow C_2H_2^{4+}(\upsilon^{-4}) + e_{A_2}. \end{aligned} \tag{8}$$

Four electrons are emitted, but the signal also appears in the three electron coincidence events of Fig. 2, when one of the photoelectrons fails to be counted due to the 70% detection efficiency. This double-photoionization process is observed in Fig. 2 in continuity with $K^{-2}V$ processes because K^{-2} DCH states can effectively be viewed as limits of $K^{-2}V$ states when the promoted K electron reaches higher and higher valence V orbitals. Finally, one also observes events located on dotted diagonal lines in Fig. 2. They reveal core-valence double-ionization paths:

$$\begin{aligned} C_2H_2 + h\nu &\rightarrow C_2H_2^{2+}(K^{-1}\upsilon^{-1}) + e_{p_1} + e_{p_2} \\ &\rightarrow C_2H_2^{3+}(\upsilon^{-3}) + e_{A_2}, \end{aligned} \tag{9}$$

where the available energy above the $K^{-2}V$ threshold is shared between the two photoelectrons.

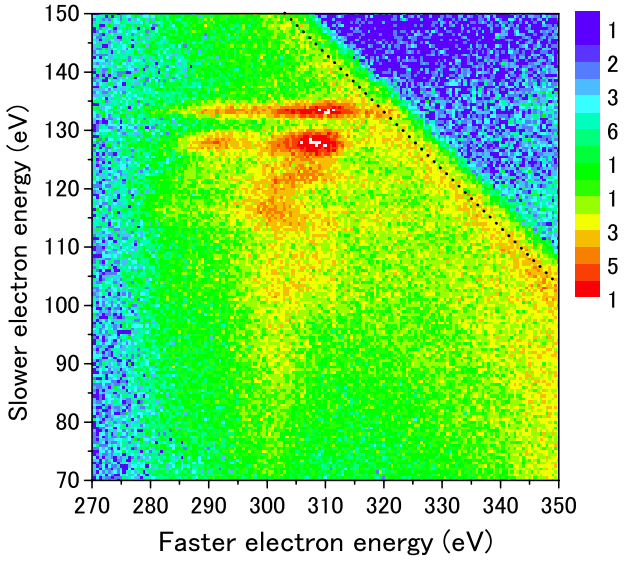

FIG. 2 (color online). Energy correlation in C_2H_2 between two electrons detected in coincidence with a third one of (200–260) eV at a photon energy of 770 eV, ~118 eV above the double core hole threshold [27]. Only three electron coincidences are considered here. Evidence for $K^{-2}V$ state formation appears in the islands at $(x, y) =$ (300 eV, 130 eV). See the text for further details.

Figure 3 compares experimental and calculated $K^{-2}V$ spectra for the molecular series C_2H_{2n}, presented as a function of the binding energy of the final ionic state. Experimental spectra on the left panels are obtained from threefold electron coincidences, as described above. For instance, the C_2H_2 spectrum is obtained by projecting the coincidence counts in the $x =$ (270–320 eV) band of Fig. 2 onto the y axis, which corresponds to the kinetic energy range of the first released Auger electron e_{A_1} in Eq. (7). The contribution of the core-valence double-ionization path (9) has been subtracted; it was estimated outside of this selected band for each $C_2H_2^{2+}$ $(K^{-1}\upsilon^{-1})$ state. Contribution from core double photoionization (8) was not subtracted. Experimental branching ratios for populating the different $K^{-2}V$ states, compared to the K^{-1} main line, were deduced from the number of recorded events, taking into account the electron detection efficiencies. Values of 0.34×10^{-3}, 0.17×10^{-3}, and 1.1×10^{-3} were obtained for peaks A in C_2H_2, A in C_2H_4, and B in C_2H_6, respectively.

Theoretical $K^{-2}V$ energy differential cross sections are reported in the right panels of Fig. 3 in absolute units (b/eV). Integrated cross sections in region A for C_2H_2 and C_2H_4, and in region B for C_2H_6, were found equal to 50, 20, and 120 b, respectively. They are in excellent agreement with values of 54, 27, and 175 b, deduced from the above-mentioned experimental branching ratios when assuming that the K^{-1} photoionization cross section in these molecules is twice that obtained for the carbon atom at a similar photon energy (2×80 kb [44]). For each

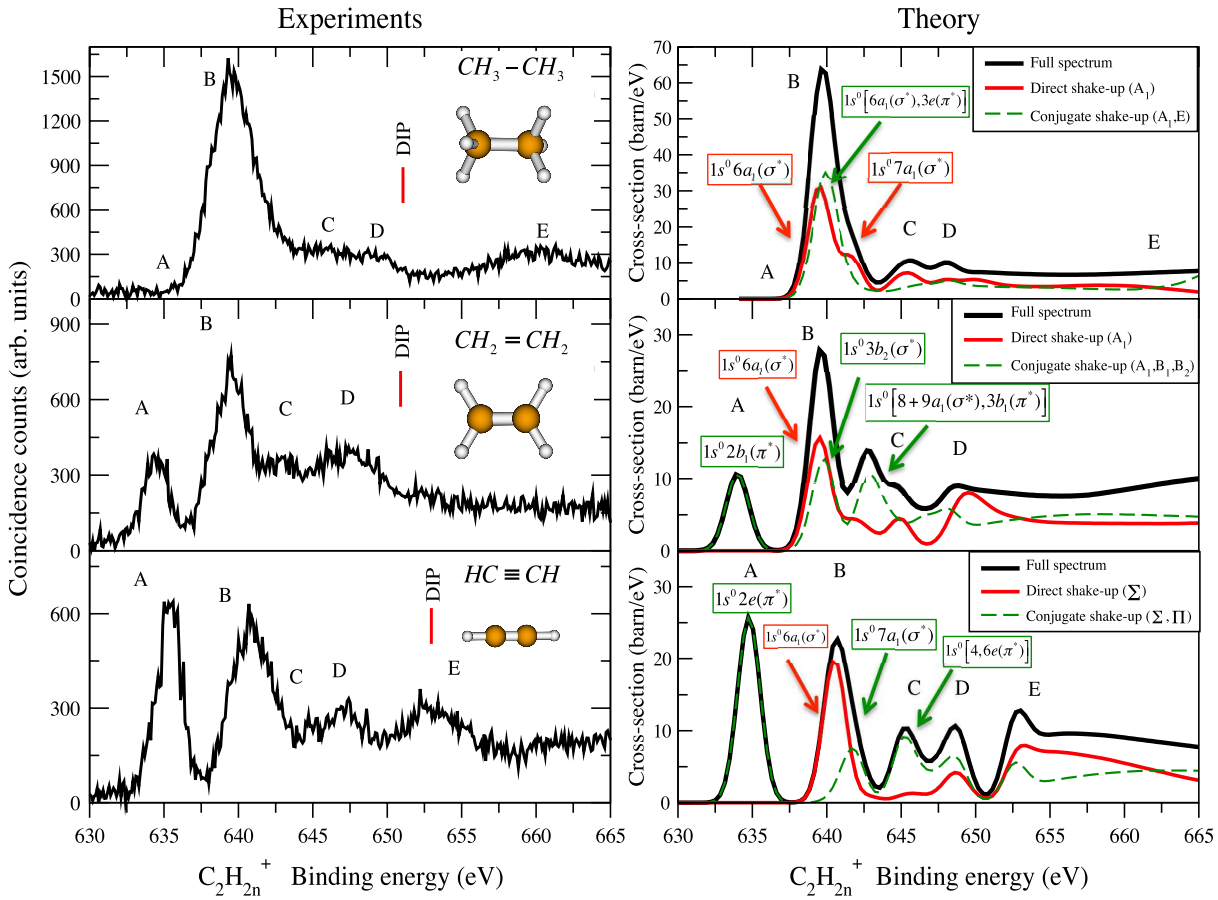

FIG. 3 (color online). Left: Experimental $K^{-2}V$ spectra recorded at a photon energy of 770 eV. The position of the core double-ionization potential (DIP) [27] is indicated. Right: Absolute theoretical $K^{-2}V$ cross sections. A convolution with a FWHM 1.8 eV Gaussian was used to simulate experimental resolution. Dashed green, solid red, and thick black lines represent, respectively, the conjugate and the direct components and their incoherent sum. Assignments are given for the main contributions.

molecule, solid (red) and dashed (green) lines designate, respectively, direct and conjugated shakeup contributions. Within the core hole localized model, group symmetries of $C_2H_2^+$, $C_2H_4^+$, and $C_2H_6^+$ are $C_{\infty v}$, C_{2v}, and C_{3v}, respectively. The selection rules imply that direct shakeup lines have all Σ or A_1 symmetry. The selection rules for conjugate shakeup lines are more complex: states in the A region are purely of Π or B_1 symmetry, while region B contains several conjugate shakeup components of Σ or A_1 and Π-(E, B_2) symmetry. Region A has a pure conjugate origin and vanishes for the C_2H_6 molecule. The B region has a mixed origin, with a major contribution from direct shakeup lines and a conjugate contribution increasing from C_2H_2 to C_2H_6. Assignments are given in the figure for the most important peaks. The thick black lines correspond to the incoherent superposition of direct and conjugate contributions.

The agreement between experiment and theory, both for peak positions and intensities, is excellent. It demonstrates important results of the present investigation. First, direct and conjugate shakeup contributions are of comparable magnitudes. The theoretical model revealed that relative intensities of direct and conjugate shakeup lines are governed by two antagonist factors. The matrix element $d_{\epsilon\ell}^{(\mu)}$ in the direct contribution is much higher (by 2 orders of magnitude) than the overlap $s_{\epsilon\ell}$ in the conjugate contribution. On the contrary, the overlap S_ℓ in the direct contribution is only nonzero thanks to minor core excited configurations of the initial ground state, as the matrix element $D_\ell^{(\mu)}$ in the conjugate part is built essentially from the dominant closed-shell configuration of the ground state. The overlap S_ℓ is then weaker (by 2 orders of magnitude) than the matrix element $D_\ell^{(\mu)}$. Second, evolution of the intensity and position of the peak observed and calculated in region A (around 635 eV) when going from acetylene (HC $\equiv$ HC) to ethylene ($H_2C=CH_2$) exhibits the same features as the main peak in conventional NEXAFS spectra observed around a photon excitation energy of 286 eV. It is slightly shifted towards lower binding energies, and its intensity decreases from acetylene to ethylene. It is attributed to a dipolar excitation to the π^* LUMO and disappears for ethane, the LUMO of which is of σ^* symmetry and located much higher in energy. These structures mimicking NEXAFS transitions and embedded in x-ray photoelectron double K-shell spectra offer the opportunity to detect specific bonds in molecules.

Third, even if Eq. (4) indicates that interference effects between direct and conjugate contributions can occur for a same symmetry of the final N state, the excellent agreement between our experimental results and the incoherent superposition confirms their weakness. This latter is dictated by propensity rules. Because the σ molecular orbital from which the electron is ejected is dominantly made of atomic s symmetry, the photoelectron coming from the direct (conjugate) process is dominantly a p (s) wave.

In summary, here is reported a combined experimental and theoretical analysis of simultaneous core hole ionization or core hole excitation ($K^{-2}V$) events in the C_2H_{2n} molecular series. It demonstrates that direct and conjugate shakeup lines are of comparable magnitude, which conveys a unique opportunity to observe a large pattern of $K^{-2}V$ states of different symmetries. In addition, computations provide absolute cross sections for weak $K^{-2}V$ events, in excellent agreement with experimental estimations.

We are grateful to the PF staff for the stable operation of the storage ring. This work was performed with the approval of the PF Program Advisory Committee (Proposal No. 2010G621). We acknowledge the interest and support of Professor Kouchi for this work and the financial support from CNRS (PICS No. 5364).

*Corresponding author.
stephane.carniato@upmc.fr

[1] K. Siegbahn *et al.*, *ESCA Applied to Free Molecules* (North-Holland, Amsterdam, 1969).
[2] J. Stöhr, *NEXAFS Spectroscopy*, Springer Series in Surface Science Vol. 25 (Springer-Verlag, Berlin, 1992).
[3] T. Åberg, Phys. Rev. **156**, 35 (1967).
[4] U. Gelius, J. Electron. Spectros. Relat. Phenom. **5**, 985 (1974).
[5] J. Berkowitz, J. L. Dehmer, Y.-K. Kim, and J. P. Desclaux, J. Chem. Phys. **61**, 2556 (1974).
[6] L. Ungier and T. D. Thomas, Phys. Rev. Lett. **53**, 435 (1984).
[7] A. Reimer, J. Schirmer, J. Feldhaus, A. Bradshaw, U. Becker, H. Kerkhoff, B. Langer, D. Szostak, R. Wehlitz, and W. Braun, Phys. Rev. Lett. **57**, 1707 (1986).
[8] M. O. Krause and C. D. Caldwell, Phys. Rev. Lett. **59**, 2736 (1987).
[9] T. Reich, P. Heimann, B. Petersen, E. Hudson, Z. Hussain, and D. Shirley, Phys. Rev. A **49**, 4570 (1994).
[10] M. Neeb, A. Kivimäki, B. Kempgens, H. Köppe, A. Bradshaw, and J. Feldhaus, Phys. Rev. A **52**, 1224 (1995).
[11] H. M. Köppe, A. L. D. Kilcoyne, J. Feldhaus, and A. M. Bradshaw, J. Electron Spectrosc. Relat. Phenom. **75**, 97 (1995).
[12] O. Hemmers, S. B. Whitfield, N. Berrah, B. Langer, R. Wehlitz, and U. Becker, J. Phys. B **28**, L693 (1995).
[13] B. Kempgens, A. Kivimaki, H. M. Koppe, M. Neeb, A. M. Bradshaw, and J. Feldhaus, J. Chem. Phys. **107**, 4219 (1997).
[14] R. L. Martin and D. A. Shirley, J. Chem. Phys. **64**, 3685 (1976).
[15] L. S. Cederbaum, and S. A. Rice, Adv. Chem. Phys. **143**, 115 (2009).
[16] C. C. Sang, D. Xiao-Bin, and D. Chen-Zhong, Chin. Phys. Lett. **25**, 3624 (2008).
[17] J. Schirmer, M. Braunstein, and V. McKoy, Phys. Rev. A **44**, 5762 (1991).
[18] G. Fronzoni, G. De Alti, and P. Decleva, J. Phys. B **32**, 5357 (1999).
[19] A. Thiel, J. Schirmer, and H. Koppel, J. Chem. Phys. **119**, 2088 (2003).
[20] K. Ueda *et al.*, Phys. Rev. Lett. **94**, 243004 (2005).
[21] R. Sankari, M. Ehara, H. Nakatsuji, A. De Fanis, H. Aksela, S. L. Sorensen, M. N. Piancastelli, E. Kukk, and K. Ueda, Chem. Phys. Lett. **422**, 51 (2006).
[22] M. Ehara, K. Kuramoto, H. Nakatsuji, M. Hoshino, T. Tanaka, M. Kitajima, H. Tanaka, A. De Fanis, Y. Tamenori, and K. Ueda, J. Chem. Phys. **125**, 114304 (2006).
[23] L. Young *et al.*, Nature (London) **466**, 56 (2010).
[24] N. Berrah *et al.*, Proc. Natl. Acad. Sci. U.S.A. **108**, 16 912 (2011).
[25] P. Salén *et al.*, Phys. Rev. Lett. **108**, 153003 (2012).
[26] P. Lablanquie *et al.*, Phys. Rev. Lett. **106**, 063003 (2011).
[27] M. Nakano *et al.*, Phys. Rev. Lett. **110**, 163001 (2013).
[28] J. H. D. Eland, M. Tashiro, P. Linusson, M. Ehara, K. Ueda, and R. Feifel, Phys. Rev. Lett. **105**, 213005 (2010).
[29] M. Mucke, J. H. D. Eland, O. Takahashi, P. Linusson, D. Lebrun, K. Ueda, and R. Feifel, Chem. Phys. Lett. **558**, 82 (2013).
[30] R. Arneberg, J. Müller, and R. Manne, Chem. Phys. **64**, 249 (1982).
[31] J. Schirmer, G. Angonoa, and L. S. Cederbaum, Z. Phys. D: At., Mol. Clusters **5**, 253 (1987).
[32] S. Carniato, and P. Millié, J. Chem. Phys. **116**, 3521 (2002); S. Carniato, Y. Luo, J. Electron Spectrosc. Relat. Phenom. **142**, 163 (2005).
[33] W. J. Hunt, and W. A. Goddard, Chem. Phys. Lett. **3**, 414 (1969).
[34] H. Ågren, V. Carravetta, L. G. M. Pettersson, and O. Vahtras, Physica (Amsterdam) **208B–209B**, 477 (1995).
[35] V. Carravetta, O. Plashkevych, and H. gren, J. Chem. Phys. **109**, 1456 (1998); Chem. Phys. **263**, 231 (2001).
[36] H. Ågren, V. Carravetta, O. Vahtras, and L. G. M. Pettersson, Theor. Chim. Acta **97**, 14 (1997).
[37] P. W. Langhoff, in *Theory and Application of Moment Methods in Many-Fermions Systems*, edited by B. J. Dalton, S. M. Grimes, J. P. Vary, and S. A. Williams (Plenum, New York, 1980), p. 191.
[38] I. Cacelli *et al.*, in *Modern Techniques in Computational Chemistry: MOTECC-91*, edited by E. Clementi (Escom, Leiden, 1991), p. 695, and references therein.
[39] D. E. Woon, and T. H. Dunning, J. Chem. Phys. **103**, 4572 (1995).
[40] K. Amemiya *et al.*, AIP Conf. Proc. **1234**, 295 (2010).
[41] J. Eland, O. Vieuxmaire, T. Kinugawa, P. Lablanquie, R. Hall, and F. Penent, Phys. Rev. Lett. **90**, 053003 (2003).
[42] K. Ito, F. Penent, Y. Hikosaka, E. Shigemasa, I. H. Suzuki, J. H. D. Eland, and P. Lablanquie, Rev. Sci. Instrum. **80**, 123101 (2009).
[43] M. Tashiro, M. Nakano, M. Ehara, F. Penent, L. Andric, J. Palaudoux, K. Ito, Y. Hikosaka, N. Kouchi, and P. Lablanquie, J. Chem. Phys. **137**, 224306 (2012).
[44] W. M. J. Veigele, At. Data Nucl. Data Tables **5**, 51 (1973).